Flow-induced separation in wall turbulence

Quoc Nguyen, Chiranth Srinivasan, and Dimitrios V. Papavassiliou*

School of Chemical, Biological and Materials Engineering, The University of Oklahoma, 100 East Boyd St., SEC T-301, Norman, Oklahoma 73019, USA

(Received 5 February 2014; revised manuscript received 26 February 2015; published 27 March 2015)

One of the defining characteristics of turbulence is its ability to promote mixing. We present here a case where the opposite happens—simulation results indicate that particles can separate near the wall of a turbulent channel flow, when they have sufficiently different Schmidt numbers without use of any other means. The physical mechanism of the separation is understood when the interplay between convection and diffusion, as expressed by their characteristic time scales, is considered, leading to the determination of the necessary conditions for a successful separation between particles. Practical applications of these results can be found when very small particles need to be separated or removed from a fluid.

DOI: 10.1103/PhysRevE.91.033019 PACS number(s): 47.27.N−, 66.10.cg

I. INTRODUCTION

Separation of particles in a flow field is important in many processes, such as biological analysis, environmental assessment, and food processing. As the number and applications of microfluidic devices increase, different separation techniques, both passive and active, have been employed not only in the laboratory but also in industry. While passive techniques only rely on the flow field and device geometry, active techniques utilize effects of external fields for better performance [1]. Some popular passive techniques are pinched flow fractionation [2–4], inertia and dean flow fractionation [5,6], membrane-based methods [7–11], and hydrodynamic filtration [12,13]. Active techniques could use electric fields [14–17], centrifugal forces [18,19], or different types of external field as in field-flow fractionation [20–23].

In most of these cases, the flows are at rather low Reynolds number. On the other side, separation of particles in turbulence has not been explored. Instead, particle transport related issues have been investigated with a focus on turbulent mixing [24–26] and particle dispersion [27–32]. This is because the fluctuating velocity in turbulence usually leads to rapid mixing, instead of separation. In this work we present the opposite, the case where particles can be separated in turbulence without using any means other than the turbulent flow field.

II. NUMERICAL METHODOLOGY

A numerical method that involves a combined direct numerical simulation (DNS) of the flow field and Lagrangian scalar tracking (LST) of mass markers is used. The pseudospectral DNS algorithm documented by Lyons *et al.* [33], and validated with experiments by Gunther *et al.* [34] is implemented. All variables are made dimensionless using the friction velocity, u^*, and the kinematic viscosity of the fluid, ν, namely, the *viscous wall units*. The dimensions of the computational box are $4\pi h \times 2h \times 2\pi h$ in the streamwise, x, normal, y, and spanwise, z, directions, respectively, where $h = 300$ is the half channel height. The computational box is meshed with $256 \times 129 \times 256$ grid points in the x, y, and z directions. The Reynolds number based on the mean centerline velocity and half of the channel height is 5,700. The channel is simulated as infinitely long in x and z and with periodic boundary conditions with periodicity lengths of $4\pi h$ and $2\pi h$, respectively. No-slip and no-penetration boundary conditions are imposed at the rigid channel walls. The fluid flowing in the channel is an incompressible Newtonian fluid with constant density and viscosity.

Scalar markers that represent mass particles are released into the flow field. These markers are passive and do not affect the flow field, an assumption that is realistic for dilute solutions. The tracking algorithm of Kontomaris *et al.* [35] is used to track individual trajectories of these markers in space and time in a Lagrangian framework, in conjunction with the DNS. The combined DNS/LST approach has been previously used to study heat transfer in high Prandtl or Schmidt number fluids [36,37]. Discussion about the accuracy of this method and comparisons of the results with experimental findings can also be found in previous publications [38–41].

Mass markers are released into the flow field after the velocity field reaches a steady, fully developed state. If $\vec{V}(\vec{x}_0,t)$ is the Lagrangian velocity of a particle that was at location $\vec{x}_0$ at time $t = t_0 = 0$, then the position $\vec{X}(\vec{x}_0,t)$ of the marker at time t is calculated based on the equation

$$\vec{V}\,(\vec{x}_0,t) = \frac{\partial \vec{X}\,(\vec{x}_0,t)}{\partial t} \tag{1}$$

At this point we make a basic assumption that a marker at any time has the velocity of the fluid particle on which it rides, which means that the relation between the Lagrangian velocity and the Eulerian velocity $\vec{U}$ is $\vec{V}(\vec{x}_0,t) = \vec{U}[\vec{X}(\vec{x}_0,t),t]$. Since the mass markers can move off a fluid particle due to molecular diffusion, the diffusion effect has been represented by adding a random walk on the marker motion after each simulation time step. The value of the diffusion step is estimated by a Gaussian distribution in each space direction with a zero mean and a standard deviation, σ, depending on the Schmidt number, Sc, ($\sigma = \sqrt{2\Delta t/\mathrm{Sc}}$) where Δt is the time step of the simulation. Multiple values of Sc are examined (Sc = 0.1, 0.7, 6, 20, 50, 100, 200, 500, 1000, 2400, 7500, 15 000, 30 000, 40 000, and 50 000) representing different substances. For each Sc, 10 000 markers are released instantaneously at the entrance of the computational box ($x = 0$). The markers are distributed with uniform spacing ($2\pi h/10\,000$) from a line

*Corresponding author: dvpapava@ou.edu

in the spanwise direction. To study the effect of the vertical position of release, markers are also released at different elevated locations, $y_0 = 0, 1, 2, 4, 5, 7, 9, 11, 13, 14, 15$ wall units away from the bottom wall.

III. RESULTS AND DISCUSSION

A. Flow-induced separation

With the term *flow-induced separation* we mean that turbulence in a flow field can be used for particle separation when different particles have different diffusivity. Previous results in our laboratory have shown that markers with lower Sc, released at the channel wall, would diffuse into the flow field faster than markers with higher Sc [40]. This effect is clearly shown in Fig. 1, in which positions of markers with Sc of 0.1 and 500 at different times are displayed. Both types of markers were released into the turbulent flow field from the bottom wall ($y_0 = 0$), at the same line ($x = 0$) and at the same time. The markers painted green are the markers with $\mathrm{Sc} = 0.1$ and the crimson markers have $\mathrm{Sc} = 500$. It is seen that the $\mathrm{Sc} = 0.1$ markers form a leading cloud, while a trailing cloud is formed by the $\mathrm{Sc} = 500$ markers. This is caused due to the differences in the diffusivity of the two types of particles. Low Sc markers have high molecular diffusivity, so they can diffuse with larger Brownian random motion jumps away from the near-wall region, where they can get convected by the larger turbulent velocity fluctuations in the y direction and by larger mean velocity in the streamwise direction. High Sc markers have low diffusivity and they cannot leave the region next to the channel wall as fast as the lower Sc markers, so they are trapped in a low velocity region for a long time.

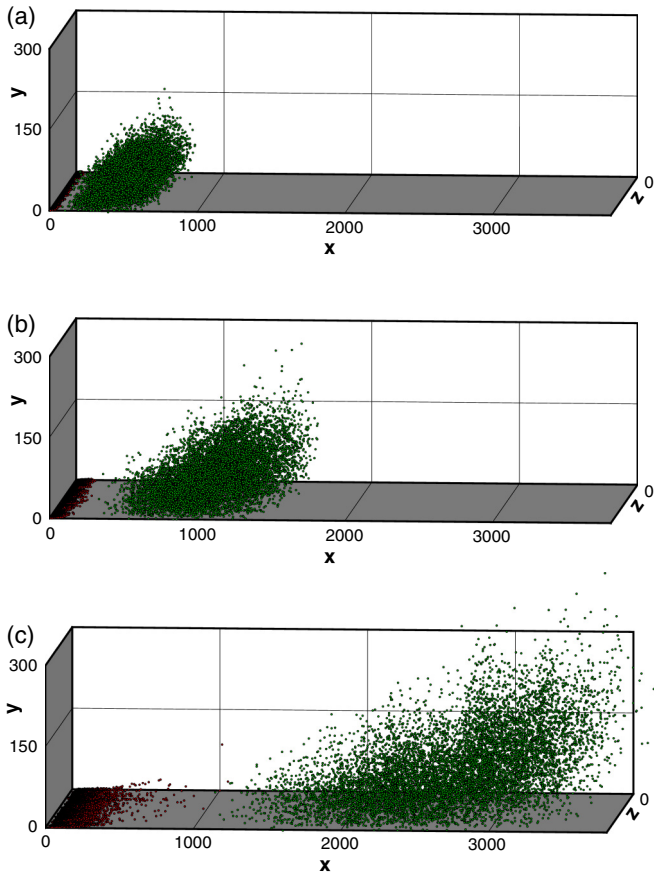

FIG. 1. (Color online) Locations of markers with $\mathrm{Sc} = 0.1$ (green) and 500 (crimson) at different times from their simultaneous release: (a) $t = 50$; (b) $t = 100$; (c) $t = 220$. Clear separation between the two clouds is observed in panel (b), while a thin overlap region is observed at $x \approx 1000$–1200 in panel (c). Only the bottom half of the channel is shown, from $y = 0$ to 300 (see Supplemental Material [42]).

At this point, it is convenient and necessary to define an *overlap region* based on the streamwise location of the clouds of markers with the two different Sc. The overlap region is the region between the slowest moving marker of the leading cloud and the fastest moving marker of the trailing cloud. The number of markers from each cloud within the overlap region can be used to quantify the separation of the two clouds. In Fig. 1, as time advances, a clear separation can be observed between the leading and the trailing clouds. Eventually, however, the trailing cloud will catch up with the leading cloud forming a short overlap region. This happens because at some point in time several markers from the trailing, high Sc cloud, will leave the viscous sublayer close to the channel wall and will start moving fast due to the turbulent mean flow, while some of the low Sc particles will diffuse back in the viscous wall region and will move slower than the rest of the particles of their type. The number of particles present in the overlap region reduces to zero when separation occurs, and becomes some finite number when the trailing cloud catches up with the leading cloud.

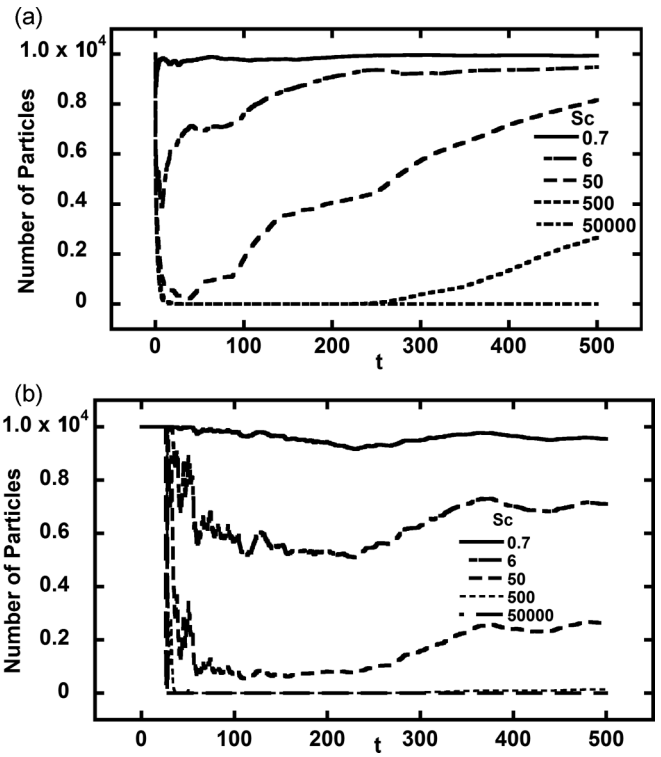

FIG. 2. Number of markers in the overlap region, N_{ov}, when markers with $\mathrm{Sc} = 0.1$ are released simultaneously with markers of different Sc. (a) Number of markers from the leading cloud, $\mathrm{Sc} = 0.1$. (b) Number of markers from the higher Sc trailing cloud.

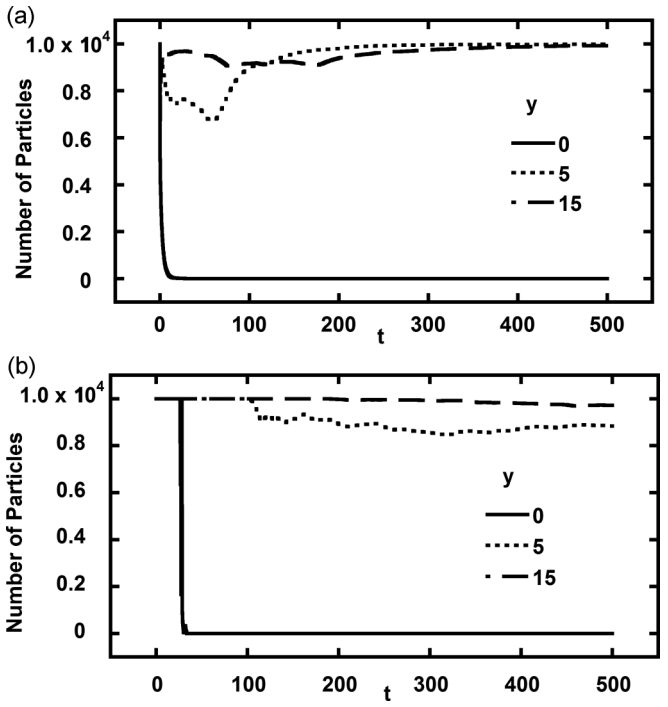

FIG. 3. Number of markers in the overlap region when markers with Sc = 0.1 and 2400 are simultaneously released at different initial vertical positions: (a) markers of the leading cloud; (b) markers of the trailing cloud.

To explore the effects of Sc on particle separation, the number of markers in the overlap region of two clouds is shown in Fig. 2 for several cases with different Sc. In all these cases, the Sc = 0.1 markers always form the leading cloud, while the trailing cloud is formed by markers with Sc = 0.7, 6, 50, 500, or 50 000. All markers are released simultaneously from the channel wall, at $y_0 = 0$. It is apparent that the two clouds with the largest Sc difference show the least number of markers in the overlap region for the longest time. As the Sc for the two clouds becomes comparable, there does not exist a time at which the overlap region disappears and separation does not occur (see Supplemental Material [42]).

Markers are also released from different sources elevated away from the wall at locations mentioned previously. In Fig. 3, we show the number of markers from the leading cloud, in (a), and trailing cloud, in (b), that are in the overlap region for markers with Sc = 0.1 and Sc = 2400 released at $y = 0, 5$, and 15. It is obvious that separation occurs most effectively when the markers are released from the wall.

B. Separation mechanism

The question that arises now is what the mechanism behind this type of separation is, and whether there is any constraint for a successful separation. Herein, we consider the two clouds to be separated if less than 0.5% of the total number of markers of any cloud (leading or trailing) is present in the overlap region. It has been shown above that if the two Sc are too close to each other, separation would not occur. In Table I, we present the minimum value of the higher Sc for each of the lower Sc in order for separation to occur. To smooth out fluctuation effects in the instantaneous flow fields, three different simulations with different initial velocity fields were used to calculate the reported results, which were determined as average values from the three runs.

The physics of why the separation occurs can be revealed when one considers the development of an instantaneous cloud of particles released in a turbulent flow field—this cloud is usually called a *puff*. Careful experiments have shown that there are different zones of development of a puff, which are distinct based on the physical mechanism of dispersion that is dominant in each zone [43,44]. Simulations have also shown that when markers are released into the flow field, they move through three stages: zone I, in which molecular diffusion dominates dispersion; zone II, which is a transition zone; and, finally, zone III, in which turbulent convection dominates dispersion. Within zone I there is a zone in which 95% of particle displacement happens because of molecular diffusion. The average time spent by markers of different Sc in this first zone, τ_{95}, and the time at which the particles move into zone III, τ_{III}, are also included in Table I, as obtained through the following empirical equations [40]:

$$\tau_{95} = 8.34 * \mathrm{Sc}^{0.38} \tag{2}$$

$$\tau_{\mathrm{III}} = 101.2 * \mathrm{Sc}^{0.35} \tag{3}$$

The ratio R_t of the τ_{III} of the low Sc over the τ_{95} of the high Sc of all successful separation cases is related to the separation time (defined as the time at which separation begins, τ_S). The correlation obtained is shown in the following equation and plotted in Fig. 4:

$$\tau_S = a * \exp\left(b * R_t^2\right) \tag{4}$$

with values of the two parameters found to be $a = 11$, $b = 2.5$.

The ratio R_t in Eq. (4) gives information about the difference of the relative motion of markers with these two Sc. It is observed that separation will happen faster if this ratio becomes smaller. If the ratio is smaller than 1 (which happens for successful separation cases), it is implied that markers with lower Sc enter zone III before the markers with higher Sc leave zone I. Turbulent convection is the dominant transport mechanism in zone III—this means that the leading cloud gets accelerated by turbulent convection before the trailing cloud exits the molecular diffusion regime. This process would cause the two clouds to separate. The two cases that have this ratio slightly larger than 1 (1.01 and 1.08) are very close to the limit for classifying a case as successful separation (99.5%

TABLE I. Summary of cases of low and high Sc, in which separation is observed using the 0.5% purity criterion. The transition times τ_{95} and τ_{III} are also presented.

Low Sc (τ_{III})	0.1 (46)	0.7 (90)	6 (190)	20 (289)	50 (398)	100 (507)
High Sc (τ_{95})	100 (48)	500 (89)	7500 (248)	15 000 (323)	30 000 (420)	40 000 (468)

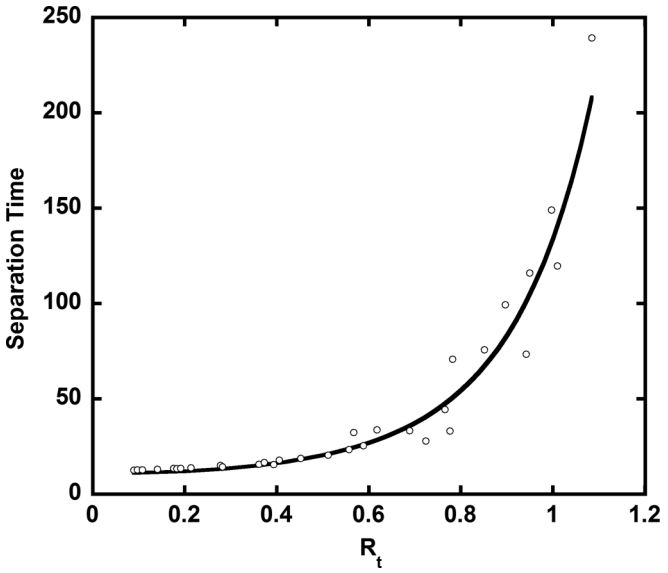

FIG. 4. Separation time as a function of the ratio R_t of the τ_{III} of the low Sc over the τ_{I} of the high Sc. The solid line is Eq. (4).

of the clouds are separated). For this study, where we defined separation as the point at which 0.5% or less of a cloud can be in the overlap region, the upper limit of R_t is 1.08. If the ratio gets higher, more markers with high Sc would leave zone I before markers with low Sc enter zone III. Because of that, more high Sc markers accelerate and catch up with the low Sc markers and the needed purity constraint will not be satisfied.

Since the times for zone transitions occur as a function of Sc in Eqs. (2) and (3), the limit 1.08 of the time zones ratio can be expressed as a relationship between the Sc of the particle cloud pairs. In order to have separation then, it is required that

$$\frac{\mathrm{Sc_{Low}}}{\mathrm{Sc_{High}}} \leqslant 0.001 * \mathrm{Sc_{High}^{0.09}} \tag{5}$$

Given the separation criterion of 0.5% and Eq. (5) as a constraint for achieving separation, this method could be employed in practice. For example, consider the separation of colloidal particles (with radii between 1 nm and 1 μm) in water at room temperature. Using the equations below [45], one can calculate the corresponding Sc of a particle with a given size, as

$$D_{AB} = \frac{\kappa T}{6\pi \mu_B R_A} \tag{6}$$

$$\mathrm{Sc} = \frac{R_A 6\pi \mu_B \nu}{\kappa T} \tag{7}$$

where D_{AB} is the diffusivity of particle A in the continuous phase B, T is the absolute temperature, κ is the Boltzmann constant, R_A is the radius of the spherical particle A, μ_B is the dynamic viscosity, and ν is the kinematic viscosity of the continuous phase. Since the Sc depends linearly on the radius, one can easily calculate the ratio of Sc, and check whether Eq. (5) is satisfied.

As an example, this method could be applied to separate viruses from red blood cells in normal saline 0.9% as the continuous phase. This is an example that is offered as a proof of concept calculation. Given that the diffusivity value of red blood cells in water is $10^{-13}(\mathrm{m^2/s})$ [46], and assuming that the viscosity and density of normal saline are equal to those of water due to very low concentration of sodium chloride, the corresponding Sc of red blood cells in saline is about 10^7. Different types of viruses, with diameters ranging from 10 to 100 nm [47], would have Sc from 23 445 to 234 450 (for instance, the diameter of HIV virus is 100 nm and the Sc is 234 450). Therefore, if a mixture of red blood cells and viruses is released in pulses into a flow field, the viruses will leave the cells behind (with the high Sc equal to 10^7). Using Eq. (5), it is obvious that some types of viruses will not satisfy the 0.5% criterion for separation. Significant separation will, however, occur in the overlap region, and then one can achieve further separation by repeating the process several times.

C. A model for particle displacement

Einstein [48] developed the following relation for molecular dispersion in a nonturbulent field $d\overline{X^2}/dt = 2D$, where D is the molecular diffusivity and X is the displacement from the source. The most influential contribution to the theory of dispersion in a turbulent field is Taylor's description of the dispersion of particles from a point source in a homogeneous, isotropic turbulence [49]. With respect to anisotropic turbulent flows, Batchelor [50] modified Taylor's theory to predict the statistical behavior of a cloud dispersed from a source in a turbulent boundary layer. We examine here whether Taylor dispersion can be used to reproduce the simulation results and whether particle separation can be predicted based on Taylor's and Batchelor's models, bypassing the need to conduct DNS and LST.

First, we examine the mean displacement of the particles in the streamwise and vertical directions. Results for selected Sc are presented in Fig. 5. It is obvious, however, that differences in the mean values of streamwise displacement should not be used alone in predicting separation with a criterion like the 0.5% criterion used above, since they only represent mean positions of the clouds without any indication of the spread of the clouds in x.

The displacement of particles in the vertical direction plays a significant role in determining streamwise velocity and position of a cloud. As previously described, particle clouds go through three different zones of development after they are released from a source at the wall. It appears that for every Sc the transition to zone III occurs when the mean cloud distance from the wall is $\bar{Y} \approx 30$. At that point, at $t = \tau_{\mathrm{III}}$, the cloud enters the zone where turbulent convection dominates the dispersion process. Identifying the proper dispersion mechanism in each zone would help build a model to predict displacement in the channel. In zone I, our earlier study found that dispersion in the direction of the velocity gradient, y, agrees well with the theory of Einstein and Taylor [40]. Since molecular diffusion is the dominant mechanism in this zone, we propose the following model for the mean vertical displacement:

$$\bar{Y} = C * \mathrm{Sc}^d t^e \qquad \text{for } t < \tau_{95} \tag{8}$$

The model contains the effect of molecular motion only. As previously discussed, the value of the diffusion step is estimated by a Gaussian distribution in each space direction with a zero mean and a standard deviation, σ, which is

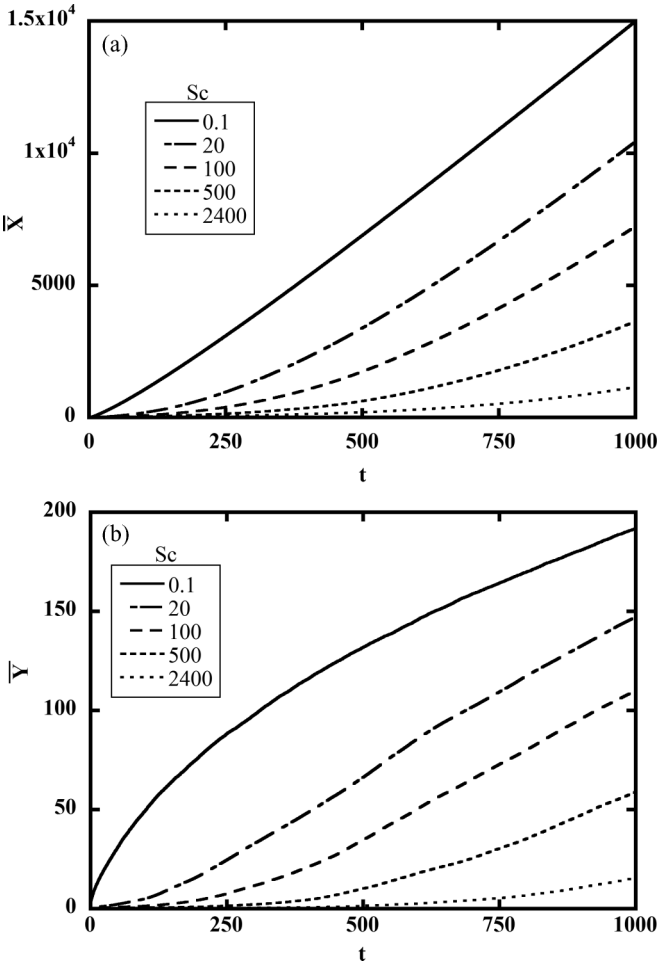

FIG. 5. Mean displacement of particles with different Sc in (a) streamwise direction; (b) vertical direction. Data obtained from LST simulations.

proportional to $\mathrm{Sc}^{-1/2}$. The exponent d in Eq. (8) can therefore be chosen to be $d = -\frac{1}{2}$. The coefficients C and e were then found to be 0.89 and 0.55, respectively, by fitting the equation with our LST data, as seen in Fig. 6.

In the case of shear flow, as is the case with our channel geometry, Batchelor suggested that the following expression can be used to predict the average motion of particles dispersing in the turbulent constant stress region [50]:

$$\bar{V} = \frac{d\bar{Y}}{dt} = b * u^* \tag{9}$$

where $b = 0.2$ should be a universal constant according to Batchelor. This expression implies that particles with different Sc will have the same mean vertical velocity. Plotting $\bar{Y}$ versus time for different Sc in the log layer region ($\bar{Y} \geqslant 30$ or $t \geqslant \tau_{\mathrm{III}}$) can be used to compare our LST data to Batchelor's prediction, as seen in Fig. 7. It is observed that particles move in the vertical direction with almost constant velocities, though particles with different Sc have slightly different velocities, and low Sc particles tend to have higher velocities initially that decreases as time increases. Because of this, we propose that the Batchelor constant b has values that depend on the Sc,

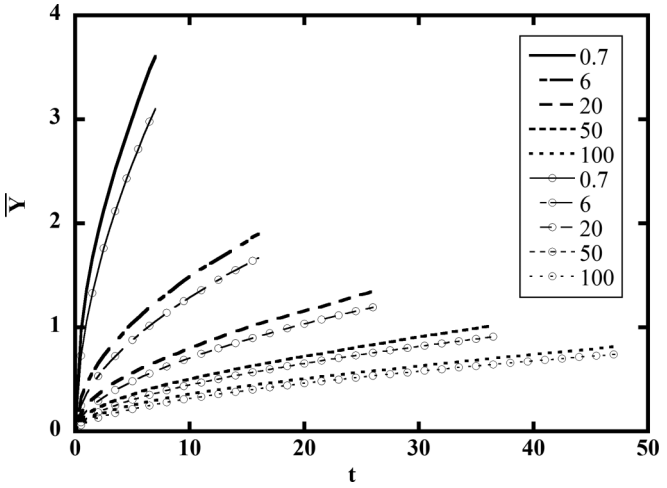

FIG. 6. Prediction of vertical displacement in zone I: comparison between the model of Eq. (9) (lines marked with open circles) and LST results (lines without any markings).

as shown in Table II. These values agree well with previously published results by different authors [51–53].

Though diffusion mechanisms of particles in the vertical direction within zone I and zone III have been identified with corresponding descriptions [Eqs. (8) and (9)], diffusion in the transition zone, starting from τ_{95} to τ_{III}, remains to be determined. Since the transition zone lies between zones I and III, we suggest the following expression to determine the vertical mean displacement for $\tau_{95} < t < \tau_{\mathrm{III}}$, based on information from zones I and III:

$$\bar{Y}_t = \bar{Y}_{t-1} + \left[\left(\frac{d\bar{Y}}{dt}\right)_{t=\tau_{95}} + \left(\frac{t-\tau_{95}}{\tau_{\mathrm{III}}-\tau_{95}}\right) * \left(b - \left(\frac{d\bar{Y}}{dt}\right)_{t=\tau_{95}}\right)\right] * \Delta t \tag{10}$$

in which b is Batchelor's constant, and Δt is the time step between times t and $(t-1)$. Using Eqs. (8)–(10) as a model, the mean vertical displacement of each Sc particle is plotted in Fig. 8 and compared with LST results. Since separation of particles happens for $t < 200$, only results up to $t = 200$ are

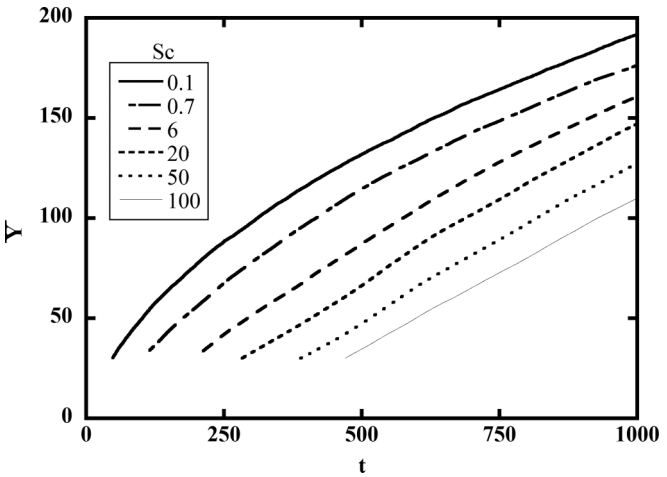

FIG. 7. Mean vertical displacement of particles in the log layer. Data obtained from LST simulation.

TABLE II. Batchelor's constant b for different Sc.

Sc	b
0.1	0.3
0.7	0.3
6	0.25
20	0.2
50 and above	0.15

plotted in Fig. 8. Reasonable agreement between our LST data and results from this model is obtained. It is worth noting that Eqs. (8)–(10) were developed based on the theories of Einstein, Taylor, and Batchelor, and this agreement encourages the use of these theories to predict mean displacement in a direction normal to the mean flow for small times.

Batchelor [50] further assumed that a constant c exists such that the mean Lagrangian velocity of a particle cloud in the streamwise direction equals the Eulerian velocity located at $c\bar{Y}$; this is due to the decrease of dU/dy with height in the channel. Based on this assumption, we have the following equation:

$$\bar{V}_x = \frac{d\bar{X}}{dt} = [\bar{U}(y)]_{y=c\bar{Y}} \tag{11}$$

It is now necessary to determine the mean velocity in the channel. Based on our DNS study, the mean flow field velocity in the channel could be described as below:

$$\begin{aligned} y \leqslant 5: &\quad U = y, \\ 5 < y \leqslant 30: &\quad U = 4.9 * \ln(y) - 3, \\ 30 < y: &\quad U = 2.6 * \ln(y) + 4.5. \end{aligned}$$

Having information of velocity in the channel and an appropriate constant c, one can use Eq. (11) to calculate $\bar{V}_x$, and thus obtain $\bar{X}$ of a particle cloud. Based on our LST data, $c = 0.6$ is the best fit, as seen in Fig. 9, and could be used in Batchelor's theory to predict mean streamwise displacement in the channel.

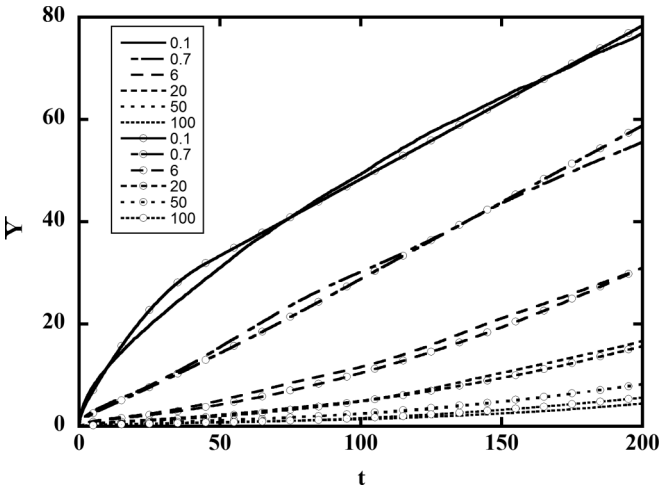

FIG. 8. Mean vertical displacement of different Sc. Results obtained from the LST data (lines without markers) and with our model based on Eqs. (8)–(10) are presented (lines marked with open circles).

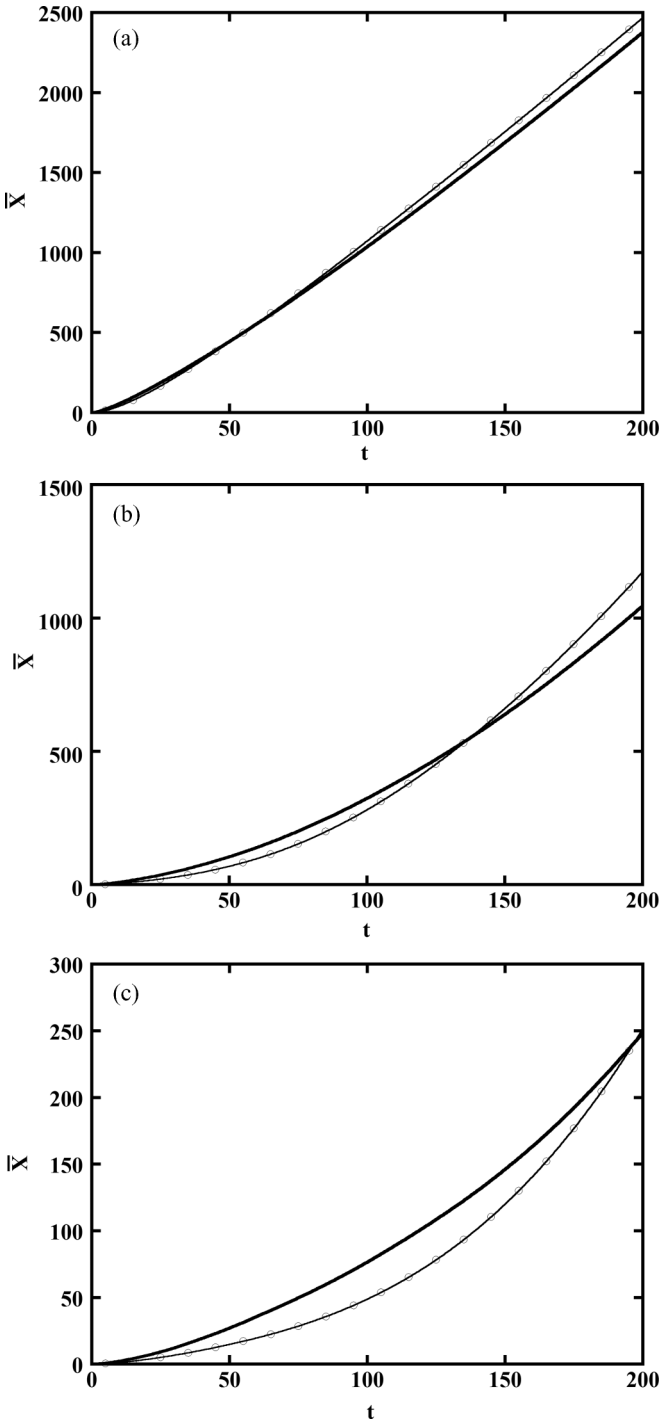

FIG. 9. Mean streamwise displacement of different Sc: (a) Sc = 0.1, (b) Sc = 6, (c) Sc = 100. Results are obtained from LST data (lined without markers) and Batchelor's model (lines marked with open circles).

At this point, it is seen that modified Taylor and Batchelor's theories produce similar results to our DNS-LST method, in terms of mean displacement in x and y directions. A further attempt is made to determine if using mean displacement as a main tool could predict separation at reasonable accuracy. However, as explained above, the mean displacement should not be used alone in predicting separation with high purity

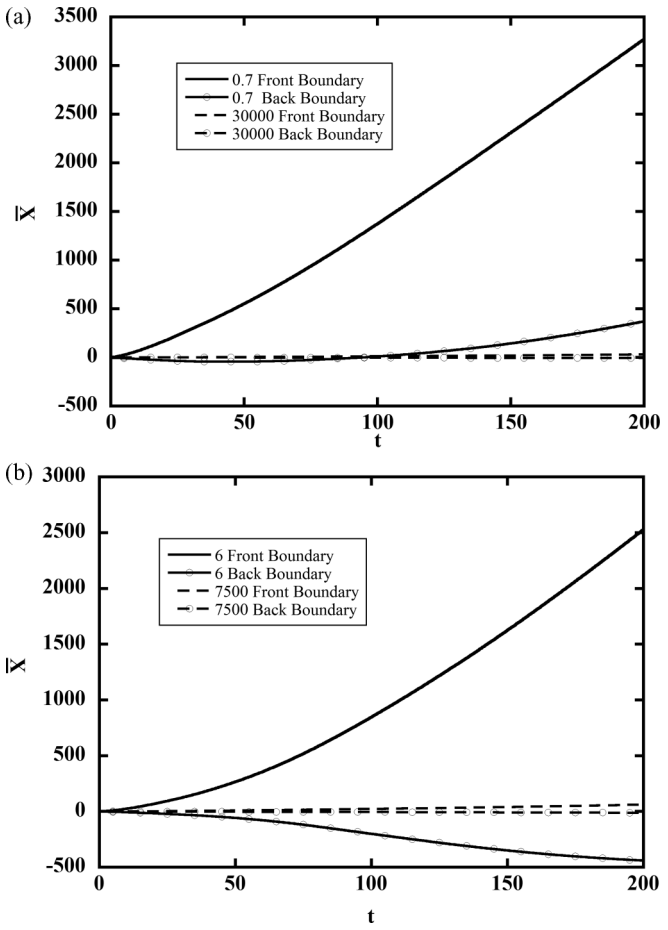

FIG. 10. Front and back boundaries of 99% of population of clouds in the streamwise direction, using mean displacement and normal distribution to predict the concentration distribution. (a) Prediction for clouds with Sc = 0.7 and 30000 and (b) prediction for clouds with Sc = 6 and 7500.

criterion. Because of turbulent velocity fluctuations the particle clouds stretch forward and backward. The stretching of the clouds also depends on molecular diffusion. We hereby define the standard deviation (STD) for the particle position in each Sc by the following expression:

$$\mathrm{STD} = \overline{(x - \bar{X})^2}^{1/2}$$

in which $\bar{X}$ represents mean location of the particle cloud that varies with time, and x indicates the location of each particle. Since no particle distribution function in x is available at this time, we assume that the concentration distribution in a particle cloud follows a normal distribution. Therefore, 99% of the particle population in the streamwise direction would lie within boundaries determined by adding and subtracting 2.5 times the STD to and from the mean streamwise displacement (which is also the cloud mean streamwise position). In Fig. 10, we plot calculations for two pairs of Sc that have been found to separate when applying the 0.5% purity criterion. For each Sc, the front and back boundaries of 99% of the population in the x direction are plotted as time increases, using $\bar{X}$ and STD from the LST data. The results indicate that clouds with Sc = 0.7 and 30 000 would not be able to separate from each other at any time earlier than 100, while that number is 512 for Sc = 6 and 7500. However, by counting the number of particles left in the overlap region, we found that Sc = 0.7 and 30 000 would separate from time equal to 14, while Sc = 6 and 7500 separate from time equal to 45. The disagreement indicates that the normal distribution is not an accurate approximation for the concentration distribution in x. One should rely on previously presented tools, i.e., Eqs. (2)–(5), to predict separation. However, the models that we developed to predict $\bar{X}$ and $\bar{Y}$ could still be used for other applications, or to predict separation, if one could obtain a more accurate particle distribution function.

IV. CONCLUSION

In this work, particles with different diffusivities, represented by passive markers with different Sc, have been found to separate from each other in turbulent flow, under certain conditions. Separation is observed when there are large differences in the particle Sc, and would occur most effectively in cases where the particles are released from sources on the channel wall. An analysis of the stages of development of puff dispersion is the explanation of the mechanism responsible for the separation. A correlation is derived to relate the time at which separation begins to the ratio of the characteristic times of development of the two clouds. This flow-induced separation can be applied to separate microscopic and nanoscopic particles with different sizes, and could be a good solution in separating very small particles especially in very dilute systems. A model, based on Batchelor's extension of the Taylor dispersion theory for shear flows, has been developed to predict mean displacement of particles with different Sc in the streamwise and vertical directions with good agreement to our LST data. It was also found that information about the mean location is not enough to predict particle separation using a high purity criterion. Instead, one should rely on the previously presented correlation to predict separation in channels. The effect of the Reynolds number on flow-induced separation needs to be examined in future work.

ACKNOWLEDGMENTS

Part of this work was done while D.V.P. was serving at the National Science Foundation (NSF). Any opinion, findings, and conclusions or recommendations expressed in this material are those of the authors and do not necessarily reflect the views of the NSF. Computations were carried out at the University of Oklahoma Supercomputing Center for Education and Research (OSCER) and using resources available through XSEDE under Project No. TG-CTS090025.

[1] P. Sajeesh and A. K. Sen, Microfluid Nanofluid **17**, 1 (2014).

[2] J. Oakey, J. Allely, and D. W. M. Marr, Biotechnol. Progr. **18**, 1439 (2002).

[3] J. Takagi, M. Yamada, M. Yasuda, and M. Seki, Lab Chip **5**, 778 (2005).
[4] M. Yamada, M. Nakashima, and M. Seki, Anal. Chem. **76**, 5465 (2004).
[5] J. S. Park and H. I. Jung, Anal. Chem. **81**, 8280 (2009).
[6] A. A. S. Bhagat, S. S. Kuntaegowdanahalli, and I. Papautsky, Phys. Fluids **20**, 101702 (2008).
[7] T. A. Crowley and V. Pizziconi, Lab Chip **5**, 922 (2005).
[8] S. G. Redkar and R. H. Davis, Am. Inst. Chem. Eng. J. **41**, 501 (1995).
[9] V. Kuberkar, P. Czekaj, and R. Davis, Biotechnol. Bioeng. **60**, 77 (1998).
[10] K. Aran, A. Fok, L. Sasso, N. Kamdar, Y. Gua, Q. Su, A. Undar, and J. Zahn, Lab Chip **11**, 2858 (2011).
[11] M. C. Lo and J. D. Zahn, *Proceedings of the 16th International Conference on Miniaturized Systems for Chemistry and Life Sciences (μTAS 2012), paper M.3.84*, edited by T. Fujii, A. Hibere, S. Takeuchi, and T. Fukuba, Chemistry & Microsystems Society, 307 (Larrel St., San Diego, CA), pp. 527–529.
[12] M. Yamada and M. Seki, Roy. Soc. Chem. **5**, 1233 (2005).
[13] M. Yamada and M. Seki, Anal. Chem. **78**, 1357 (2006).
[14] X.-B. Wang, J. Yang, Y. Huang, J. Vykoukal, F. F. Becker, and P. R. C. Gascoyne, Anal. Chem. **72**, 832 (2000).
[15] O. Gaal, *Electrophoresis in the Separation of Biological Macromolecules* (Wiley, New York, 1980), p. 422.
[16] P. R. C. Gascoyne and J. Vykoukal, Electrophoresis **23**, 1973 (2002).
[17] Z. R. Gagnon, Electrophoresis **32**, 2466 (2011).
[18] L. J. Gimbert, P. M. Haygarth, R. Beckett, and P. J. Worsfold, Environ. Sci. Technol. **39**, 1731 (2005).
[19] S. Juen, K. Uberbacher, J. Baldauf, K. F. Lamprecht, R. Tessadri, R. Lackner, and R. A. Hopfel, Superlattices Microstruct. **11**, 181 (1992).
[20] J. C. Giddings, J. Chem. Educ. **50**, 667 (1973).
[21] J. C. Giddings, Science **260**, 1456 (1993).
[22] J. C. Giddings, F. J. F. Yang, and M. N. Myers, Science **193**, 1244 (1976).
[23] A. Lenshof and T. Laurell, Chem. Soc. Rev. **39**, 1203 (2010).
[24] L. Valiño, C. Dopazo, and J. Ros, Phys. Rev. Lett. **72**, 3518 (1994).
[25] B. I. Shraiman and E. D. Siggia, Phys. Rev. Lett. **77**, 2463 (1996).
[26] J. Schumacher and K. R. Sreenivasan, Phys. Rev. Lett. **91**, 174501 (2003).
[27] M. K. Rivera and R. E. Ecke, Phys. Rev. Lett. **95**, 194503 (2005).
[28] S. Ott and J. Mann, J. Fluid Mech. **422**, 207 (2000).
[29] W. H. Snyder and J. L. Lumley, J. Fluid Mech. **48**, 41 (1971).
[30] C. Beck, Phys. Rev. Lett. **98**, 064502 (2007).
[31] M. Bourgoin, N. T. Ouellette, H. Xu, J. Berg, and E. Bodenschatz, Science **311**, 835 (2006).
[32] M. Chaves, G. Eyink, U. Frisch, and M. Vergassola, Phys. Rev. Lett. **86**, 2305 (2001).
[33] S. L. Lyons, T. J. Hanratty, and J. B. McLaughlin, Int. J. Numer. Methods Fluids **13**, 999 (1991).
[34] A. Gunther, D. V. Papavassiliou, M. D. Warholic, and T. J. Hanratty, Exp. Fluids **25**, 503 (1998).
[35] K. Kontomaris and T. J. Hanratty, J. Comput. Phys. **103**, 231 (1992).
[36] C. Srinivasan and D. V. Papavassiliou, Phys. Fluids **23**, 115105 (2011).
[37] A. K. Karna and D. V. Papavassiliou, Phys. Fluids **24**, 035102 (2012).
[38] D. V. Papavassiliou and T. J. Hanratty, Int. J. Heat Mass Transf. **40**, 1303 (1997).
[39] D. V. Papavassiliou, Int. J. Heat Mass Transf. **45**, 3571 (2002).
[40] D. V. Papavassiliou, Int. J. Heat Fluid Flow **23**, 161 (2002).
[41] C. Srinivasan and D. V. Papavassiliou, Ind. Eng. Chem. Res. **50**, 8881 (2011).
[42] See Supplemental Material at http://link.aps.org/supplemental/10.1103/PhysRevE.91.033019 for full animations of the cloud motion.
[43] D. J. Shlien and S. Corrsin, Int. J. Heat Mass Transf. **19**, 285 (1976).
[44] M. Poreh and J. E. Cermak, Int. J. Heat Mass Transf. **7**, 1083 (1964).
[45] R. B. Bird, W. E. Stewart, and E. N. Lightfoot, *Transport Phenomena*, 2nd ed. (Wiley, New York, 2006), p. 532.
[46] H. C. Berg, *Random Walks in Biology* (Princeton University Press, Princeton, NJ, 1993), p. 60.
[47] R. A. Harvey, P. C. Champe, and B. D. Fisher, *Microbiology* (Lippincott Williams & Wilkins, New York, 2007), p. 3.
[48] A. Einstein, Ann. Phys. **17**, 549 (1905).
[49] G. I. Taylor, Proc. London Math. Soc. **20**, 196 (1922).
[50] G. K. Batchelor, Arch. Mech. Stosow. **3**, 661 (1964).
[51] J. E. Cermak, J. Fluid Mech. **15**, 49 (1963).
[52] R. C. Malhotra and J. E. Cermak, J. Geophys. Res. **68**, 2181 (1963).
[53] J. W. Deardorff, Bound.-Lay. Meteorol. **5**, 451 (1974).